

# Grid Adaptation for the Dirichlet–Neumann Representation Method and the Multiscale Mixed Finite-Element Method

Knut-Andreas Lie · Jostein R. Natvig · Stein Krogstad · Yahan Yang · Xiao-Hui Wu

Received: date / Accepted: date

**Abstract** A Dirichlet–Neumann representation method was recently proposed for upscaling and simulating flow in reservoirs. The DNR method expresses coarse fluxes as linear functions of multiple pressure values along the boundary and at the center of each coarse block. The number of flux and pressure values at the boundary can be adjusted to improve the accuracy of simulation results, and in particular to resolve important fine-scale details. Improvement over existing approaches is substantial especially for reservoirs that contain high permeability streaks or channels. As an alternative, the multiscale mixed finite-element (MsMFE) method was designed to obtain fine-scale fluxes at the cost of solv-

ing a coarsened problem, but can also be used as upscaling methods that are flexible with respect to geometry and topology of the coarsened grid. Both methods can be expressed in mixed hybrid form, with local stiffness matrices obtained as 'inner products' of numerically computed basis functions with fine-scale sub-resolution. These basis functions are determined by solving local flow problems with piecewise linear Dirichlet boundary conditions for the DNR method and piecewise constant Neumann conditions for MsMFE. Adding discrete pressure points in the DNR method corresponds to subdividing faces in the coarse grid and hence increasing the number of basis functions in the MsMFE method. The methods show similar accuracy for 2D Cartesian cases, but the MsMFE method is more straightforward to formulate in 3D and implement for general grids.

---

K.-A. Lie  
SINTEF ICT, P.O. Box 124 Blindern, N0-0314 Oslo, Norway  
Tel.: +47-22067710  
Fax: +47-22067350  
E-mail: Knut-Andreas.Lie@sintef.no

J. R. Natvig  
SINTEF ICT  
Tel.: +47-21609612  
E-mail: jnatvig@slb.com  
*Present address:* Schlumberger Information Solutions, Aslakveien 14E, NO-0753 Oslo, Norway

S. Krogstad  
SINTEF ICT  
Tel.: +47-22067714  
Fax: +47-22067350  
E-mail: Stein.Krogstad@sintef.no

Y. Yang  
ExxonMobil Upstream Research Company  
Tel.: +1-713-431-6350  
Fax: +1-713-431-4138  
E-mail: yahan.yang@exxonmobil.com

X.-H. Wu  
ExxonMobil Upstream Research Company  
Tel.: +1-713-431-4748  
Fax: +1-713-431-4138  
E-mail: xiao-hui.wu@exxonmobil.com

**Keywords** Coarsening · upscaling · Dirichlet-Neumann representation · multiscale mixed finite elements

## 1 Introduction

Being able to understand and predict flow and transport processes is decisive to enhance the recovery from hydrocarbon reservoirs. Porous rocks are typically highly heterogeneous and exhibit a multiscale behavior in the sense that small-scale flow paths determine the macro-scale displacement of fluids in a reservoir. Describing all pertinent flow processes with a single model is impossible. Flow modeling is therefore divided into separate steps according to physical scales: from rock models on the micro scale, via facies models and geological models, to simulation models on the macro scale. Upscaling is inevitable to transfer parameters and effective properties up in the model hierarchy.

Herein, we focus on upscaling from geological models to simulation models. To accurately model heterogeneous

rock formations, geo-cellular models typically have complex geometries and topologies and may contain millions of cells. Even for models with a few tens or hundred thousand cells, a typical forward simulation will require hours of computer time. Coarsening the grid and upscaling petrophysical parameters is therefore a necessary step to reduce model sizes and reduce the turnaround time for workflows that utilize simulations. When geological models are coarsened, the blocks in the resulting simulation model can be quite large and may encompass important geological variations. The upscaled models are obviously easier to simulate, but are also only approximations of the original model. Errors introduced in the upscaling process can be large, in particular for models that describe high-contrast media. A critical technical challenge is to reduce simulation times while maintaining a high degree of accuracy for the simulations.

To this end, several methods have been proposed. In the Dirichlet–Neumann representation (DNR) method [20], expressions for flow rates are derived as linear functions of the pressure value at the center and at multiple discrete pressure points along the faces of each coarse block. The number of pressure points at the boundary is flexible and may be chosen to provide an adequate representation of pressure profiles and flow distribution throughout a dynamical simulation. In the multiscale mixed finite-element (MsMFE) method [7], one constructs a set of special basis functions that incorporate local effects of fine-scale heterogeneity into a global coarse-scale flow problem. The basis functions are computed by solving localized flow problems driven by source terms. The DNR and MsMFE methods are similar in the sense that both allow straightforward reconstruction of fine-scale flow solutions and can hence be used as part of a multiscale computational procedure. On the other hand, the methods can be seen as complementary: whereas the basis functions in the MsMFE method are localized and determined by specifying Neumann boundary conditions on fluxes, the local flow solutions in the DNR method are determined by specifying Dirichlet boundary conditions for the pressure.

The purpose of the paper is two-fold. First, we extend the DNR method from Cartesian to fully unstructured grids in 2D; extension to simple 3D grids is discussed in [17]. To extend DNR, we borrow ideas from the MsMFE method, write the DNR method on mixed hybrid form and notice that adding pressure points corresponds to subdividing coarse faces, and hence increasing the number of basis functions, in a MsMFE method. Second, we compare the accuracy and robustness of the DNR method and two versions of the MsMFE method (the one-block and two-block formulation) and investigate how errors induced by the artificial boundary conditions that localize the computation of basis functions and Dirichlet–Neumann maps can be reduced by subdividing interfaces between coarse blocks, e.g., to adapt to heterogeneities in the permeability field. In particular, we investigate:

- if the methods can reproduce constant flow fields when subdividing coarse faces, i.e., consistency;
- the sensitivity of the methods with respect to the aspect ratio of grid cells;
- how the presence of different permeability contrasts affects the precision of the methods; and
- if different strategies of *a posteriori* subdivisions of faces in cells where the pressure maximum principle is not satisfied can help improve the robustness of the methods.

## 2 Grid and discretization

We consider the following single-phase flow problem

$$v + K\nabla p = 0, \quad \nabla \cdot v = q, \quad (1)$$

for  $x \in \Omega$ . Here,  $K$  is the permeability tensor,  $v$  is the fluid velocity,  $p$  is the fluid pressure, and  $q$  represents sources and sinks. In addition, (1) needs to be augmented with boundary conditions on  $\partial\Omega$ .

To discretize (1), we partition  $\Omega$  into a set of  $N_\Omega$  non-overlapping polyhedral grid cells. Each cell  $\Omega_i$  has  $n_i$  planar polyhedral faces  $\Gamma_{ik}$ , and we set  $N = \sum_i n_i$ . The set of polyhedral cells form a conformal unstructured grid in the sense that each of the  $N_F$  internal faces connects two grid cells only. The parameters of (1) are constant on each grid cell. Let  $\mathbf{v}_i$  denote the vector of outward fluxes on  $\Omega_i$  and  $p_i$  and  $\pi_i$  the pressures at the cell and face centers, respectively. Discretization methods used for (1) in reservoir simulation are typically constructed to be locally conservative and exact for linear solutions. Such schemes can be written in a form that uses Darcys law to relate the three quantities  $\mathbf{v}_i$ ,  $p_i$ , and  $\pi_i$  through a matrix of *one-sided transmissibilities*  $\mathbf{T}_i$  associated with a single cell,

$$\mathbf{v}_i = \mathbf{T}_i(\mathbf{e}p_i - \pi_i), \quad (2)$$

where  $\mathbf{e}$  is an  $n_i \times 1$  vector of ones and  $\mathbf{T}_i$  is assumed to be positive definite. Different choices of  $\mathbf{T}_i$  result in different methods like the standard two-point flux-approximation scheme, the mixed finite-element method, the related mimetic finite difference schemes, and (in a certain sense) some multipoint flux approximations; this is discussed in more detail, e.g., in [14, 19]. For a two-point scheme, for instance, standard transmissibilities associated with the connection between two cells can be derived from (2) by assuming continuity of fluxes and face pressures, giving the relation  $v_{ij} = T_{ij}(p_i - p_j)$ .

Extending (2) with flux continuity at cell faces and mass conservation, we obtain the global system in mixed-hybrid form

$$\begin{bmatrix} \mathbf{T}^{-1} & \mathbf{C} & \mathbf{D} \\ \mathbf{C}^T & \mathbf{0} & \mathbf{0} \\ \mathbf{D}^T & \mathbf{0} & \mathbf{0} \end{bmatrix} \begin{bmatrix} \mathbf{v} \\ -\mathbf{p} \\ \pi \end{bmatrix} = \begin{bmatrix} \mathbf{0} \\ \mathbf{q} \\ \mathbf{0} \end{bmatrix}. \quad (3)$$

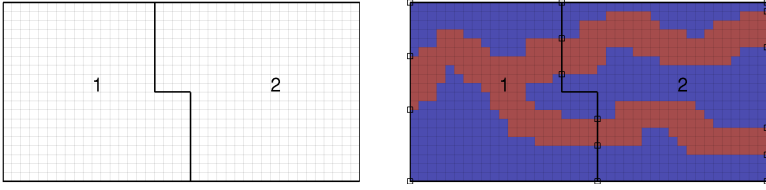


**Fig. 1** Two coarse blocks formed by amalgamation of fine cells. In the right plot, the coarse interfaces have been subdivided to better represent strong permeability contrasts, e.g., assuming that red color represents cells with high permeability and blue color cells with low permeability.

Here,  $\mathbf{v}$  is the stacked vector of cell fluxes,  $\mathbf{p}$  denotes the cell pressures, and  $\boldsymbol{\pi}$  is the vector of interface pressures with one value per face. In the system matrix,  $\mathbf{T}$  is the  $N \times N$  matrix  $\text{diag}(\mathbf{T}_1, \dots, \mathbf{T}_{N_\Omega})$ ,  $\mathbf{C}$  is the  $N \times N_\Omega$  matrix  $\text{diag}(\mathbf{e}_1, \dots, \mathbf{e}_{N_\Omega})$ , and  $\mathbf{D}$  is the  $N \times N_\Gamma$  matrix with a single unit entry in each row identifying the interface corresponding to the entry in  $\mathbf{v}$ . In Sections 3 and 4, we will see that the DNR and MsMFE methods can be written in the form (3) on the coarse scale, using basis functions to evaluate the entries in the  $\mathbf{T}$  matrix.

In the following, we will operate on a coarse grid consisting of blocks that are formed by amalgamating cells from an underlying fine grid. The interface between two coarse blocks may or may not have been subdivided into multiple faces (see Figure 1); either way, each coarse face consists of a (connected) set of cell faces from the underlying grid. To simplify the presentation, we keep the notation from the fine grid and let the coarse grid consist of  $N_\Omega$  coarse grid blocks  $\{\Omega_i\}$  and  $N_\Gamma$  coarse interfaces  $\{\Gamma_j\}$ , defined so that each block  $\Omega_i$  is a simply connected set of (fine) grid cells and each coarse interface  $\Gamma_j$  is a connected set of fine-grid faces forming (part of) the interface between two coarse blocks or (part of) the outer boundary of a single coarse block.

### 3 The Dirichlet–Neumann Representation Method

A Dirichlet–Neumann operator maps the values of a Dirichlet (pressure) boundary condition of the solution of the elliptic pressure equation (1) in a closed domain to the values of a Neumann (flux) condition. To reduce the error induced by artificial boundary conditions in traditional upscaling methods, [20] recently proposed to use such maps to derive fluxes as linear functions of multiple discrete pressure values along the boundary of each coarse block and pressure value at the center of the block. The number of pressure values at a block boundary can be varied, and by adapting the pressure points, and adequate representation of pressure profiles and flux distributions during simulation can be obtained by adapting the pressure points to features in the fine-scale geology. Herein, we will extend the Dirichlet–Neumann Representation (DNR) method from 2D Cartesian to 2D unstructured grids; extension to simple 3D grids are discussed in [17].

To define a discrete Dirichlet–Neumann map for a coarse block  $\Omega_i$  with boundary  $\partial\Omega_i$  formed by  $n_i$  coarse interfaces  $\Gamma_{i_k}$ , one first introduces a partition of unity  $\{g_{i_k}\}$  on the interface and then computes a set of shape functions  $\psi_{i_k}$  de-

fined on the fine grid restricted to  $\Omega_i$ . Assuming that  $g_{i_k}$  is nonzero Dirichlet on a segment of  $\partial\Omega_i$ , the corresponding shape function reads,

$$\psi_{i_k} + K\nabla\phi_{i_k} = 0, \quad \nabla \cdot \psi_{i_k} = 0, \quad (4)$$

in  $\Omega_i$  with  $\phi_{i_k} = g_{i_k}$  on  $\partial\Omega_i$ . We will come back to how the functions  $g_{i_k}$  are defined later.

For each shape function  $\psi_{i_k}$ , we define a vector  $\mathbf{m}_k$  with elements  $m_{k\ell} = \int_{\Gamma_{i_k}} \psi_{i_k} dS$ . Once all the local equation (4) have been solved, the  $n_i$  discrete shape functions can be collected as columns in a matrix  $\mathbf{M}_i = (\mathbf{m}_1, \dots, \mathbf{m}_{n_i}) \in \mathbf{R}^{n_i \times n_i}$  such that

$$\mathbf{v}_i = \mathbf{M}_i \boldsymbol{\pi}_i. \quad (5)$$

Since each column of  $\mathbf{M}_i$  in (5) is obtained from a solution of the homogeneous equation (4),  $\mathbf{e}^\top \mathbf{M}_i$  is the zero vector and the matrix  $\mathbf{M}_i$  has rank  $n_i - 1$ . To represent flow in coarse blocks containing source terms, (5) needs to be expanded by interface fluxes  $\mathbf{m}_i$  from a non-homogeneous shape function. We compute the effect of source terms in  $\Omega_i$  by solving

$$\psi_{i_0} + K\nabla\phi_{i_0} = 0, \quad \nabla \cdot \psi_{i_0} = \begin{cases} 1/|\Omega_i|, & \text{if } q = 0 \text{ in } \Omega_i \\ q/\int_{\Omega_i} q, & \text{otherwise,} \end{cases} \quad (6)$$

with homogeneous Dirichlet boundary conditions. (For  $q = 0$ , one can use a different source term, e.g., as discussed in [4]). The outward fluxes on the interfaces of  $\partial\Omega_i$  are then evaluated to form the vector  $\mathbf{m}_i$ . When source terms are included, we get the expression  $\mathbf{v}_i = \mathbf{M}_i \boldsymbol{\pi}_i + \mathbf{m}_i q_i$  for the outfluxes of block  $\Omega_i$ , where  $q_i = \int_{\Omega_i} q$ .

To approximate the solution of (1), we require continuity of the flux across all coarse-grid interfaces. Let  $\mathbf{v}$  be the  $N \times 1$  stacked vector of all outward-directed block interface fluxes  $\mathbf{v}_i$ , where  $N = \sum_{i=1}^{N_\Omega} n_i$ . Furthermore, if we collect the Dirichlet–Neumann maps of all coarse blocks in a  $N \times N$  block-diagonal matrix  $\mathbf{M}$ , the non-homogeneous flux vectors in an  $N \times N_\Omega$  matrix  $\mathbf{m}$ , and let  $\boldsymbol{\pi}$  be the vector of all coarse-grid interface pressures, we may write the linear system as

$$\begin{bmatrix} \mathbf{I} & -\mathbf{M}\mathbf{D} \\ \mathbf{D}^\top & \mathbf{0} \end{bmatrix} \begin{bmatrix} \mathbf{v} \\ \boldsymbol{\pi} \end{bmatrix} = \begin{bmatrix} \mathbf{m}\mathbf{q} \\ \mathbf{0} \end{bmatrix}, \quad (7)$$

where  $\mathbf{q}$  is the vector of source terms per block. Each row in the  $N \times N_\Gamma$  matrix  $\mathbf{D}$  has a single non-zero entry equal one such that  $\mathbf{D}\boldsymbol{\pi}$  are the interface pressures in a block-wise ordering. This implies that  $\mathbf{D}^\top \mathbf{v}$  is the vector of sums of

the approximations to each interface flux. For internal interfaces, this sum should be zero to ensure flux continuity on the coarse grid, whereas for outer interfaces the flux should either be zero or equal any Neumann conditions imposed on the system. With a simple manipulation of (7), we get a linear system for the interface pressures

$$\mathbf{D}^\top \mathbf{M} \mathbf{D} \boldsymbol{\pi} = -\mathbf{D}^\top \mathbf{m} \mathbf{q}. \quad (8)$$

**Mixed-Hybrid Formulation.** Equation (7) can be written in mixed-hybrid form (3) if we define a suitable interpretation of the coarse pressure  $p_i$  and the transmissibility matrix  $\mathbf{T}_i$  so that (2) is fulfilled for each block  $\Omega_i$ . In particular, by multiplying (2) from left by  $\mathbf{e}^\top$ , we get  $q_i = \mathbf{e}^\top \mathbf{v}_i = \mathbf{e}^\top \mathbf{T}_i (\mathbf{e} p_i - \boldsymbol{\pi}_i)$ , from which we eliminate  $p_i$

$$p_i = \frac{1}{\mathbf{e}^\top \mathbf{T}_i \mathbf{e}} (\mathbf{e}^\top \mathbf{T}_i \boldsymbol{\pi}_i + q_i).$$

Substituting this expression back into (2), we obtain

$$\mathbf{v}_i = - \underbrace{\left( \mathbf{T}_i - \frac{1}{\mathbf{e}^\top \mathbf{T}_i \mathbf{e}} \mathbf{T}_i \mathbf{e} \mathbf{e}^\top \mathbf{T}_i \right)}_{\mathbf{M}_i} \boldsymbol{\pi}_i + \underbrace{\frac{1}{\mathbf{e}^\top \mathbf{T}_i \mathbf{e}} \mathbf{T}_i \mathbf{e}}_{\mathbf{m}_i} q_i. \quad (9)$$

Here, we have indicated which parts must be equal to  $\mathbf{M}_i$  and  $\mathbf{m}_i$ , respectively, for the method to be equivalent to the DNR method as defined above. By substitution and using the relations  $\mathbf{M}_i \mathbf{e} = \mathbf{M}_i^\top \mathbf{e} = \mathbf{0}$  and  $\mathbf{e}^\top \mathbf{m}_i = 1$ , it can be verified that

$$\mathbf{T}_i = -\mathbf{M}_i + \frac{1}{\alpha_i} \mathbf{m}_i \mathbf{w}_i^\top$$

represents a family of transmissibility matrices equivalent to the DNR method, where  $\mathbf{w}_i$  is a weighting vector ( $\mathbf{e}^\top \mathbf{w}_i = 1$ ) and  $\alpha_i$  is a scaling parameter. For homogeneous media and blocks with planar faces, the resulting method will be consistent independently of  $\alpha_i$ . In practice, however, it is important to keep the condition number of  $\mathbf{T}_i$  reasonable and  $\alpha_i$  can be used for this purpose. A good choice for  $\alpha_i$  depends on the choice of units. For a given  $\mathbf{w}_i$  and  $\alpha_i$ , the relation between the block and interface pressures is given by  $p_i = \mathbf{w}_i^\top \boldsymbol{\pi}_i + \alpha_i q_i$ . Herein, we will use  $\mathbf{w}_i = \mathbf{e}/(\mathbf{e}^\top \mathbf{e})$  or  $\mathbf{w}_i = \mathbf{m}_i$  and  $\alpha_i = 1/[\text{darcy}] \approx 1.0132 \cdot 10^{12}$ . Another natural choice for  $\alpha_i$  is by setting it equal to the average of  $\Psi_{i_0}$  from (6). This is justified by setting  $\mathbf{v}_i = \mathbf{m}_i$  and  $\boldsymbol{\pi}_i = \mathbf{0}$  into (2), to obtain  $\mathbf{m}_i = \mathbf{T}_i \mathbf{e} p_i = \frac{1}{\alpha_i} \mathbf{m}_i \mathbf{w}_i^\top \mathbf{e} p_i = \frac{p_i}{\alpha_i} \mathbf{m}_i$ .

**Boundary conditions.** The choice of boundary conditions used to construct local solutions of (1) in flow-based upscaling can have a significant impact on the accuracy. To construct a discrete Dirichlet–Neumann map for a grid block  $\Omega_i$  with  $n_i$  coarse interfaces, we need  $n_i$  linearly independent functions  $g_k : \partial\Omega_i \rightarrow \mathbf{R}$  that will be used as Dirichlet conditions for (4). In [20] it was shown that the DNR method produces accurate results when each  $g_k$  is a piecewise linear function in the curve length  $s$  measured along  $\partial\Omega_i$  (from

some reference) with joints at  $n_i$  points on  $\partial\Omega_i$ . These points are referred to as *pressure points*. In general, the accuracy of the method can be improved by adjusting the number and position of pressure points.

In [20], pressure points are specified along  $\partial\Omega_i$  according to a rule that accounts for permeability variation and partitions the boundary into a set of non-overlapping interfaces defined so that there is one pressure point on each interface  $\Gamma_j$ . Some technical conditions ensure that this partition is uniquely defined. Assuming that  $s_j$  is the value of the curve length in the pressure point (centroid) of  $\Gamma_j$ , we require that  $g_k(s_j) = \delta_{jk}$  to ensure that the basis functions  $\{g_k\}$  form a partition of unity on  $\partial\Omega_i$ , which is necessary for the Dirichlet–Neumann method to give zero flux for constant-pressure solutions. Furthermore, by choosing the pressure points as degrees-of-freedom for the interface pressure, the matrix  $\mathbf{M}_i$  is easily constructed from the interface fluxes of each shape function.

Herein, we have chosen a different approach: we take the partition of  $\partial\Omega_i$  as given and choose the centroid of a fine-grid face in the middle of the coarse interface as the pressure point of interface  $\Gamma_j$ . This enables the use of grid amalgamation techniques (see e.g., [9, 10]) to define the interfaces in the coarse grid, and is straightforward to extend to 3D. More details are given in [17].

#### 4 The Multiscale Mixed Finite-Element Method

The main idea of the MsMFE method [7, 5] is to construct a special approximation space defined over the coarse grid. This is done by computing basis functions that represent the flow between two neighboring grid blocks and solve a local flow problem of the form (6), but with different boundary conditions used for localization. Two types of boundary conditions will be presented below, giving two MsMFE methods with somewhat different behavior. Unlike the DNR method, the MsMFE methods are designed to give conservative fluxes directly on the coarse and fine grid, but conservative fluxes can also be reconstructed on any intermediate grid using the fine-scale resolution of the basis functions.

**One-block basis.** An MsMFE basis function represents the flow over an interface or sub-interface  $\Gamma_k$  between two neighboring blocks. Restricted to one block  $\Omega_i$ , the basis function  $\psi_{i_k}$  is defined as the solution of

$$\psi_{i_k} + K \nabla \phi_{i_k} = 0, \quad \nabla \cdot \boldsymbol{\psi}_{i_k} = \boldsymbol{\omega}_i, \quad (10)$$

with Neumann boundary conditions  $\boldsymbol{\psi}_{i_k} \cdot \mathbf{n} = \mathbf{v}_k$  on  $\Gamma_k$  and  $\boldsymbol{\psi}_{i_k} \cdot \mathbf{n} = 0$  on  $\partial\Omega_i \setminus \Gamma_k$ , see [2, 3]. The basis functions are normalized by requiring that  $\int_{\Omega_i} \boldsymbol{\omega}_i = 1$  and  $\int_{\Gamma_k} \mathbf{v}_k = 1$ . If *global* information is available as a previously computed flux field  $\mathbf{v}_0$ , this is incorporated in  $\mathbf{v}_k$  by setting  $\mathbf{v}_k = \mathbf{v}_0 \cdot \mathbf{n}_k / \int_{\Gamma_k} \mathbf{v}_0 \cdot \mathbf{n}_k ds$ . If global information is available, we

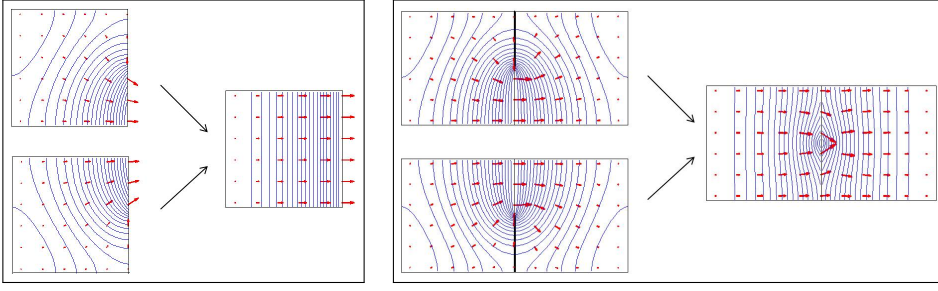


**Fig. 2** The left plot shows two one-block MsMFE basis functions for a subdivided interface as well as the sum of the two basis functions reproducing *half* of a Raviart–Thomas basis function, and hence linear pressure drop. The right plot shows two two-block MsMFE basis functions for a subdivided interface as well as the sum of the two that fails to reproduce constant flow fields.

set  $v_k = 1/|\Gamma_k|$ . Multiple degrees-of-freedom per interface can be obtained by subdividing the interface and assigning one basis function to each subsurface. The computation of each basis remains the same: simply setting non-zero flux conditions on the sub-interface and zero flux conditions elsewhere. To the left in Figure 2, we have depicted two basis functions corresponding to a subdivided interface (with constant non-zero flux conditions) for a homogeneous domain. Taking the average of these functions we obtain the basis function for the original non-divided interface.

**Two-block basis.** In the two-block approach [1,4], the basis function for an interface  $\Gamma_k$  between blocks  $\Omega_i$  and  $\Omega_j$  is defined as the solution of

$$\psi_k + K\nabla\phi_k = 0, \quad \nabla \cdot \psi_k = \begin{cases} \omega_i, & \text{for } \mathbf{x} \in \Omega_i, \\ -\omega_j, & \text{for } \mathbf{x} \in \Omega_j \end{cases} \quad (11)$$

in  $\Omega_i \cup \Omega_j$  with zero Neumann boundary on  $\partial(\Omega_i \cup \Omega_j)$ . If  $\Gamma_k$  is a subset of the interface between  $\Omega_i$  and  $\Omega_j$ , a zero Neumann condition is imposed as an *inner boundary condition* on the remaining part of the interface ( $\partial\Omega_i \cap \partial\Omega_j \setminus \Gamma_k$ ). To the right in Figure 2, we have depicted two basis functions corresponding to a subdivided interface for a homogeneous domain. Because of the inner boundary, the flux field has a peak (singularity) at the inner corner. This means that the normal component of the flux over the open boundary is varying strongly and nonlinearly, and that the average of the two basis functions differs from the basis function defined for the original non-divided interface, and cannot represent constant flow fields [6].

**The multiscale method.** To approximate the solution of (1), we introduce the multiscale expansion

$$\mathbf{v}_{fs} = \Psi\mathbf{v} + \tilde{\mathbf{u}}_{fs}, \quad \mathbf{p}_{fs} = \mathbf{I}\mathbf{p} + \tilde{\mathbf{p}}_{fs}, \quad \pi_{fs} = \mathbf{J}\pi + \tilde{\pi}_{fs}. \quad (12)$$

Here,  $(\mathbf{v}, \mathbf{p}, \pi)$  denote unknowns associated with the coarse grid, whereas  $(\mathbf{v}_{fs}, \mathbf{p}_{fs}, \pi_{fs})$  denote the same quantities reconstructed on the fine grid. The matrix  $\Psi$  represents the fine-scale reconstruction operator for fluxes and contains the basis functions  $\psi_{i_k}$  (or  $\psi_k$ ). The matrices  $\mathbf{I}$  and  $\mathbf{J}$  are simple prolongation operators from coarse blocks and coarse faces to cells and faces in the fine grid, respectively. Finally,  $\tilde{\mathbf{u}}_{fs}$ ,  $\tilde{\mathbf{p}}_{fs}$ , and  $\tilde{\pi}_{fs}$  denote reminder terms defined on the fine grid. To form a global system on the coarse grid  $\{\Omega_i\}$ , we

insert (12) into (3), multiply by the compression operator  $\text{diag}(\Psi^T, \mathbf{I}^T, \mathbf{J}^T)$  from the left, and drop all remainder terms

$$\begin{bmatrix} \Psi^T \mathbf{T}^{-1} \Psi & \Psi^T \mathbf{C} \mathbf{I} & \Psi^T \mathbf{D} \mathbf{J} \\ \mathbf{I}^T \mathbf{C}^T \Psi & \mathbf{0} & \mathbf{0} \\ \mathbf{J}^T \mathbf{D}^T \Psi & \mathbf{0} & \mathbf{0} \end{bmatrix} \begin{bmatrix} \mathbf{v} \\ -\mathbf{p} \\ \pi \end{bmatrix} = \begin{bmatrix} \mathbf{0} \\ \mathbf{I}^T \mathbf{q} \\ \mathbf{0} \end{bmatrix}. \quad (13)$$

**MsMFE as an upscaling method.** To use MsMFE as an upscaling method, all we need to do is compute inverse transmissibility matrices  $\mathbf{T}_i^{-1}$  that consist of ‘inner products’ of the basis functions  $\psi_{i_k}$  on the corresponding coarse blocks  $\Omega_i$ . As above, the inverse transmissibility matrix  $\mathbf{T}_i^{-1}$  describes the relation between the fluxes and the block and interface pressures through (2). Given basis functions  $\psi_{i_k}$ , the  $(k, \ell)$  entry of matrix  $\mathbf{T}_i^{-1}$  is given by

$$\mathbf{T}_i^{-1}(k, \ell) = \int_{\Omega_i} \psi_{i_k} \cdot \mathbf{K}^{-1} \psi_{i_\ell}.$$

The elements of  $\mathbf{T}_i^{-1}$  can equivalently be derived from the computed pressure at the boundary  $\partial\Omega_i$ . First, observe that the pressure  $\phi_{i_k}$  in (10) is only defined up to a constant and we therefore have to add a condition, such as e.g.,  $\int_{\Omega_i} \omega_i \phi_{i_k} = 0$ , to close the equation. Using Gauss–Green’s formula, we derive

$$\begin{aligned} \mathbf{T}_i^{-1}(k, \ell) &= \int_{\Omega_i} \psi_{i_k} \cdot \mathbf{K}^{-1} \psi_{i_\ell} = - \int_{\Omega_i} \psi_{i_k} \cdot \nabla \phi_{i_\ell} \\ &= - \int_{\Omega_i} \nabla \cdot \psi_{i_k} \phi_{i_\ell} + \int_{\partial\Omega_i} \phi_{i_\ell} \psi_{i_k} \cdot \mathbf{n} \\ &= - \int_{\Omega_i} \omega_i \phi_{i_\ell} + \int_{\Gamma_k} \phi_{i_\ell} v_k = \int_{\Gamma_k} \phi_{i_\ell} v_k. \end{aligned} \quad (14)$$

This means that  $\mathbf{T}_i^{-1}(k, \ell)$  is the  $(v_k$ -weighted) average of the pressure basis  $\phi_{i_\ell}$  on interface  $k$ . In particular,  $\mathbf{T}_i^{-1} = [\phi_{i,1}, \dots, \phi_{i,n_i}]$ , where  $\phi_{i,k}$  is the vector of average interface pressures in the numerical solution of (10).

## 5 Numerical experiments

In this section, we report the results of several numerical experiments that were conducted to verify, validate, and compare the three numerical methods presented above (DNR, 1-block MsMFE, and 2-block MsMFE). First, we discuss two basic properties, reproduction of constant flow fields

and sensitivity with respect to aspect ratios. Second, we use the SPE10 data set to investigate the robustness of the methods and how subdivision of coarse-block interfaces affects the accuracy of the methods. Third, we discuss how the accuracy of the methods can be improved by carefully adapting the coarse grid to high-contrast media that contain barriers, high-flow channels, or combinations thereof. All experiments were conducted using the MATLAB Reservoir Simulation Toolbox [14, 16].

### 5.1 Constant flow fields

Reproduction of constant flow fields is often used as a basic design principle for discretization and streamline-tracing methods. By design, the DNR method does not automatically reproduce constant flow unless the coarse-grid faces are subdivided in certain ways. Likewise, the 2-block version of the MsMFE method will not reproduce linear pressure correctly if the coarse-grid interfaces are subdivided, as was illustrated in Figure 2. On the other hand, the 1-block version of MsMFE and the 2-block version with no face refinement will correctly reproduce constant flow for homogeneous, isotropic permeability.

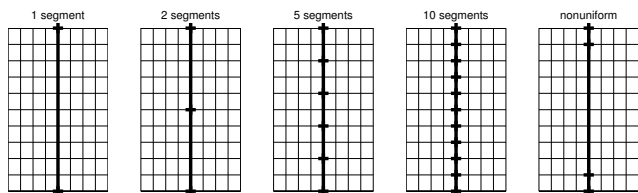


Fig. 3 Subdivision of a single coarse face in Example 1.

*Example 1 (Cartesian grid)* To investigate this in more detail, we use a simple setup consisting of a square  $50 \text{ m} \times 50 \text{ m}$  domain with a pressure drop from 150 to 50 bar from the west to the east boundary, giving an analytical solution  $p(x, y) = 150 - 2x$ . We consider a  $50 \times 50$  Cartesian fine grid partitioned uniformly into  $5 \times 5$  coarse blocks. Each interface between two blocks is subdivided as shown in Figure 3. Table 1 reports errors in the pressure for a homogeneous, isotropic permeability computed by the DNR and the two MsMFE methods. For comparison, the table also reports the corresponding errors for a model with lognormal permeability, for which neither of the schemes will reproduce the correct flow unless refined to the fine grid. Figure 4 plots approximate solutions in the homogeneous case computed on a grid with two segments per coarse face. The figure also lists the computed fluxes out of the four boundaries. It is obvious that the DNR method fails to reproduce the constant flow field in the homogeneous case. However, we observe that adding extra segments at the corners of the coarse grid

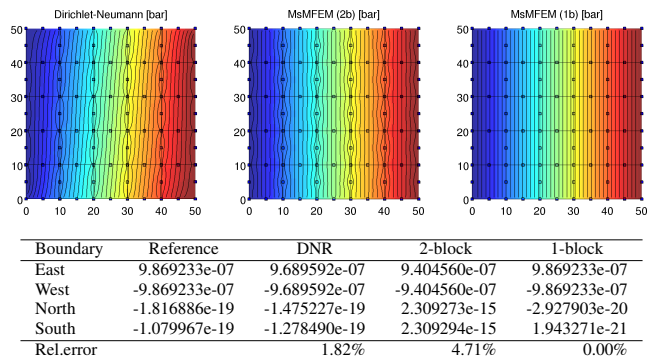


Fig. 4 Pressures and fluxes across the outer boundary for the constant flow example on a  $5 \times 5$  coarse grid in which all coarse faces have been subdivided into two segments of equal length. The dots signify the ends of the face segments.

enables the method to reproduce constant flow in the homogeneous case, and reduces the error by one order of magnitude for the cost of three times as many basis functions for the lognormal case. For short, we will use the term DNR-c to refer to the method with this type of nonuniform subdivision in the following. For isotropic permeabilities, the 2-block MsMFE method reproduces constant flow if coarse faces are not subdivided. However, dividing the faces into two or three segments gives a significant increase in the error, as expected. On the other hand, although this method is not a consistent discretization, it produces (by far) the lowest error when using no face refinement for the lognormal permeability. The 1-block method produces constant flow by design in the homogeneous, isotropic case. Finally, we remark that all three methods produce results to machine precision when the coarse faces (but not the blocks) are refined down to the fine grid.

Unstructured grids will naturally impose coarse faces that do not follow the axial directions. The next example investigates what effect this has on the solution quality.

*Example 2 (PEBI grid)* We consider the exact same setup as in the previous example, but now using a 2D unstructured perpendicular bisector (PEBI) grid. We construct two different coarse grids, an almost uniform grid obtained by sampling from a  $5 \times 5$  Cartesian partition and a k-way Metis partition [15] with 25 blocks, and conduct a convergence study on a sequence of increasing face refinements for the two grids. Figure 5 shows four grids and reports errors in coarse-scale fluxes computed by the DNR and the two MsMFE methods. As should be expected, the errors of the DNR and the 1-block methods decay with increasing face refinement. The error in the 1-block method is particularly high because the basis functions are constructed by imposing constant flux along coarse faces that do not align with the principal axis of flow. For DNR, we do not apply the DNR-c fix since partitions with obtuse angles have no natural corners,

**Table 1** Errors in coarse fluxes measured in the relative  $L^1$  norm for a pressure drop over a 2D reservoir with homogeneous or lognormal permeability represented on a  $50 \times 50$  grid. The approximate solutions are computed on a coarse  $5 \times 5$  grid in which each face is subdivided into  $n$  equal segment or three nonuniform segments with lengths one, eight, and one cells.

Segments	bases	Homogeneous			Lognormal		
		DNR	2-block	1-block	DNR	2-block	1-block
1	60	1.04e-01	1.50e-13	1.62e-13	9.68e-02	1.59e-02	4.66e-02
2	120	2.47e-02	9.01e-02	1.40e-13	2.51e-02	9.93e-02	5.38e-02
5	300	8.97e-02	3.16e-02	1.67e-13	8.87e-02	3.47e-02	2.28e-02
10	600	1.05e-13	6.25e-13	2.05e-13	6.51e-14	1.12e-12	3.41e-13
nonuniform	180	7.96e-14	4.77e-02	1.60e-13	8.83e-03	5.72e-02	5.31e-02

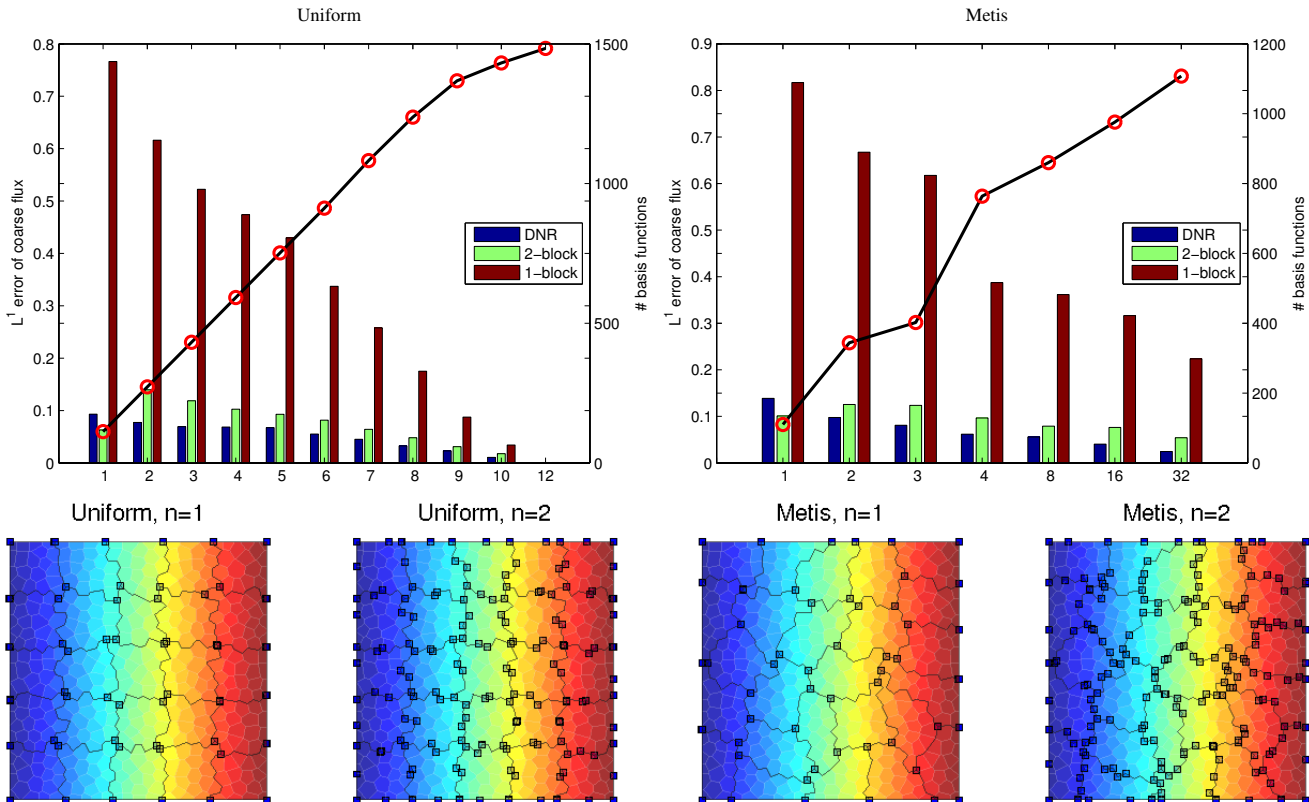


**Fig. 5** Constant flow for an unstructured PEBI grid for a homogeneous medium. The bar plots show  $L^1$  errors of the coarse-scale fluxes whereas the line plots show the number of coarse blocks involved in the construction of basis functions. The left column shows results for an almost uniform  $5 \times 5$  coarse grid with face refinement derived from a  $5n \times 5n$  Cartesian grid. The right column shows results for a  $25n$ -block coarse grid generated by Metis with face refinement derived from a  $25n$ -block Metis partition.

as was the case in the previous example; see also the discussion of wrap-around effects after Example 3. For the 2-block method, the error *increases* significantly when the coarse faces are subdivided and we need to introduce a quite fine subdivision before the error comes back to the level of the base case, in particular with the uniform partition. Results for a set of lognormal permeabilities are qualitatively the same and thus not reported.

## 5.2 Sensitivity to aspect ratio

Real-life reservoir models typically have grids with high and large variations in aspect ratios. It is therefore important to

have a method that is robust to changes in aspect ratios. In the next example, we therefore investigate how the accuracy of the DNR, DNR-c and the two MsMFE methods is affected by increasing the aspect ratio of the cells in the underlying fine grid.

*Example 3 (Aspect ratio)* We consider a  $100 \times (100/L)$  m<sup>2</sup> domain with homogeneous permeability, subject to two different boundary conditions: linear pressure making a  $\pi/3$  degree angle with the  $x$ -axis or Dirichlet boundary conditions with pressure  $p(s) = 1000 \sin(\pi s)$  on the north and east faces (assuming that these are parametrized by  $s \in [0, 1]$ ) and zero pressure otherwise. Table 2 reports errors for aspect ratios  $L = 1, 2, 3, 4, 6, 12$ . The DNR method has significantly

**Table 2** Errors in coarse-scale fluxes measured in the relative  $L^1$  norm for a 2D reservoir of dimensions  $100 \times (100/L)$  with flow driven by two different boundary conditions. Approximate solutions are computed on a  $12 \times 12$  coarse grid overlying a fine  $60 \times 60$  grid.

Ratio	Linear, $\pi/3$ angle				Analytic			
	DNR	DNR-c	2-block	1-block	DNR	DNR-c	2-block	1-block
1:1	8.46e-02	3.00e-13	1.63e-09	2.94e-13	8.71e-02	3.11e-03	4.95e-03	4.95e-03
2:1	2.53e-01	2.02e-13	1.32e-09	2.03e-13	2.30e-01	3.47e-03	7.71e-03	7.71e-03
3:1	3.29e-01	3.18e-13	1.10e-09	3.12e-13	3.05e-01	4.39e-03	1.03e-02	1.03e-02
4:1	3.66e-01	1.82e-13	9.15e-10	1.76e-13	3.45e-01	5.46e-03	1.31e-02	1.31e-02
6:1	4.02e-01	3.50e-13	6.70e-10	3.39e-13	3.90e-01	8.06e-03	1.79e-02	1.79e-02
12:1	4.40e-01	2.06e-13	3.60e-10	1.87e-13	4.41e-01	1.21e-02	2.60e-02	2.60e-02

larger errors than the three other methods and the error increases with increasing aspect ratio. The error also increases for the MsMFE methods for analytic boundary conditions, but this can mainly be attributed to inaccurate representation of the Dirichlet boundary conditions; if we subdivide all boundary faces, the error does not increase with increasing aspect ratio. Overall, the DNR-c method is the most accurate, but also has three times as many basis functions as the MsMFE methods.

Without subdivision of coarse-block faces, the Dirichlet-Neumann maps in the DNR method are constructed by imposing a unit pressure at the midpoint of one coarse face and zero pressures at the other face midpoints. For Cartesian grids, this gives a wrap-around effect at the coarse-grid vertices. Since each map will be constructed based on a pressure drop along *both axial directions*, one effectively introduces a coupling of the flow in the axial directions. This wrap-around effect causes the error to increase significantly with increasing aspect ratios. Introducing extra degrees of freedom at the corners (in the form of segments that are one cell wide) breaks the coupling between the axial directions and makes the DNR method robust with respect to aspect ratios. We believe that this observation can also shed some light into another method that has not been discussed herein: In the multiscale finite-volume (MsFV) method [12], each basis function is constructed much in the same way as in DNR, by imposing a unit pressure at one vertex of a dual coarse block and zero at the others. Hence, it is likely that the loss of accuracy for increasing aspect ratios observed for the MsFV method is caused by a similar wrap-around effect.

### 5.3 *A posteriori* subdivision

So far, we have only presented highly idealized test cases that highlight certain features of the DNR and MsMFE methods. To get a more challenging, and somewhat more realistic test case, we consider Model 2 from the 10th SPE Comparative Solution Project [8], which was designed to benchmark various upscaling methods and has later become a popular data set when validating multiscale methods. The most common test in the literature is to use horizontal slices with

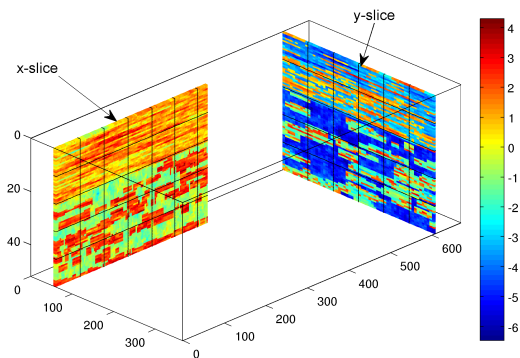


**Fig. 6** Logarithm of permeability on vertical slices of the SPE10 data set:  $x$ -slice shows lateral permeability,  $y$ -slice shows vertical permeability.

isotropic permeability. We have performed systematic studies of slices extracted along all three axial directions, subject to linear and analytic conditions as discussed above. In all simulations, face refinement is imposed *a priori* without the use of information about flow patterns, either as a subdivision into equal segments or as a nonuniform subdivision that seeks to separate high and low permeability values into different face segments, e.g., as illustrated in the right plot of Figure 1, which we will refer to as permeability thresholding. Altogether, the results are somewhat inconclusive and cannot be used to claim that one method, or subdivision strategy, is better than the other, but generally show that both the DNR and the 2-block MsMFE methods are able to represent the subgrid effects of the strongly heterogeneous and channelized permeability to produce accurate flow fields for most slices. However, there are also isolated cases for which the methods give quite high errors. As a possible remedy, we consider a simple approach for *a posteriori* adaption: Knowing that the analytical solution should be monotone, we can refine coarse faces and recompute the corresponding basis functions in regions where the approximate solution falls outside the minimum and maximum values from the prescribed boundary condition.

*Example 4 (SPE10)* To investigate the effect of a *a posteriori* face adaption as a possible remedy, we consider two types of vertical slices from the SPE10 data set: 60  $x$ -slices with

120 × 80 cells and 220  $y$ -slices with 60 × 80 cells. When sampling vertical slices, correlations that mostly run in the lateral direction of the model are cut off, giving very patchy permeability fields, as can be seen in Figure 6. These challenging permeabilities have been selected on purpose to provoke non-monotone behavior in our numerical methods. To drive flow, we specify linear boundary conditions with  $p = 150$  bar on the west and  $p = 50$  bar on the east boundary of each 2D slice or analytic boundary conditions with  $p(s) = 1000\sin(\pi s)$  on the north and east boundaries (assuming these are parametrized by  $s \in [0, 1]$ ) and zero pressure otherwise. As base cases before refinement, we use a 6 × 8 grid for the  $x$ -slices or a 12 × 8 grid for the  $y$ -slices. To these base grids, we apply five different types of *a priori* refinement of each face:

- subdivision in two or three segments;
- subdivision using permeability threshold values 10, 100, or 1000 mD.

After an approximate fine-scale solution has been computed on any of these grids, we use the following three different strategies to impose a *a posteriori* refinement of faces (illustrated in Figure 7):

- block:** refine the coarse faces down to the fine grid for all blocks that have a coarse-scale pressure outside the range of the prescribed boundary conditions;
- cell:** add extra faces for those cells along the boundary that have reconstructed fine-scale pressure outside the prescribed range;
- >n%:** refine coarse faces down to the fine grid for all blocks in which more than  $n\%$  of the cells have reconstructed pressures outside the prescribed pressure range.

In the following we will use the relative  $L^1$  error of the coarse fluxes as a measure of solution quality for approximate solutions computed by the DNR method. The left column of Figure 8 shows errors after *a priori* face refinement for each layer versus the error on the corresponding base grid (without face refinement). For dots *below* the line  $y = x$ , the *a priori* face refinement has lowered the error, and in most cases to less than unity. However, we notice that in a few cases the refinement *increases* the error, in particular if faces are subdivided into three segments. The middle column shows similar plots of errors obtained by also including a *a posteriori* refinement. Here, we notice that introducing a *a posteriori* refinements directly on the base grid will in most cases not reduce the error significantly (and hence the black points are clustered around the line  $y = x$ ). However, if we first do an *a priori* face refinement and then an *a posteriori* refinement, the error is reduced and below unity in most cases. In the right column, we compare the efficiency of the different approaches by plotting the mean error over all slices as a function of the mean number of basis functions.

For both the  $x$  and  $y$ -slices, using either an *a priori* subdivision into two equal segments, or a permeability threshold of 100 mD, are the two most efficient strategies. Moreover, using an *a posteriori* refinement indicator based on cells gives lower error, but also more basis functions, than using an indicator based on blocks. Similar results were observed for  $x$ -slices with linear pressure and  $y$ -slices with analytic boundary conditions. Finally, we notice that a *a posteriori* adaption can, of course, also be introduced in a similar manner for the MsMFE methods.

#### 5.4 High contrast media

Extensive numerical experiments show that even though multiscale methods may provide high accuracy for media with strong permeability contrasts (barriers or streaks with high permeability) [4, 18], one can also easily construct cases for which the methods fail to provide accurate solutions [13, 4]. Previous experience has shown that adapting the coarse grid to barriers in the permeability field may give improved resolution [4].

*Example 5 (Barrier/high-flow cases)* In this example, we consider a rectangular domain that either contains barriers in a high-permeable background, or high-permeable streaks in a low-permeable background. Three-dimensional permeability realizations are generated by extruding three different 50 × 50 background/foreground masks to ten vertical layers:

- Mask 1: isolated objects representing barriers or streaks on a constant background; each object is at least three cells wide.
- Mask 2: isolated objects that are so thin that many of the internal connections within the object is across vertices rather than faces in the 2D mask.
- Mask 3: objects that cross each other and hence form longer barrier/high-flow regions; each object is at least two cells wide.

The three masks are shown in the left column of Figure 9.

To study the effect of permeability contrasts on the 2-block MsMFE method, we keep the high-permeable feature in each problem fixed at 1 D and vary the low permeability seven orders of magnitude,  $10^{-6}, \dots, 1$  D. Flow is driven by Dirichlet boundary conditions equal 300 bar on the south side and 100 bar on the north side. Altogether, this gives  $2 \times 3 \times 7$  different flow cases. For each flow case, we consider six different grids,

- a uniform  $5 \times 5 \times 1$  coarse grid (base grid);
- a volumetric refinement of the base grid in which contiguous regions of foreground permeability form extra blocks (denoted 'vNUC');

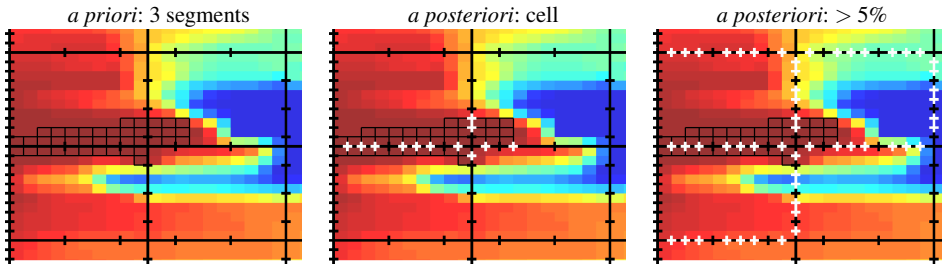


**Fig. 7** *A posteriori* refinement of grid. The left figure shows the initial grid, with cells that violate the pressure conditions outlined with thin lines. The middle and right plots show a *a posteriori* refinement using two different strategies, with the endpoints of new intervals marked in white.

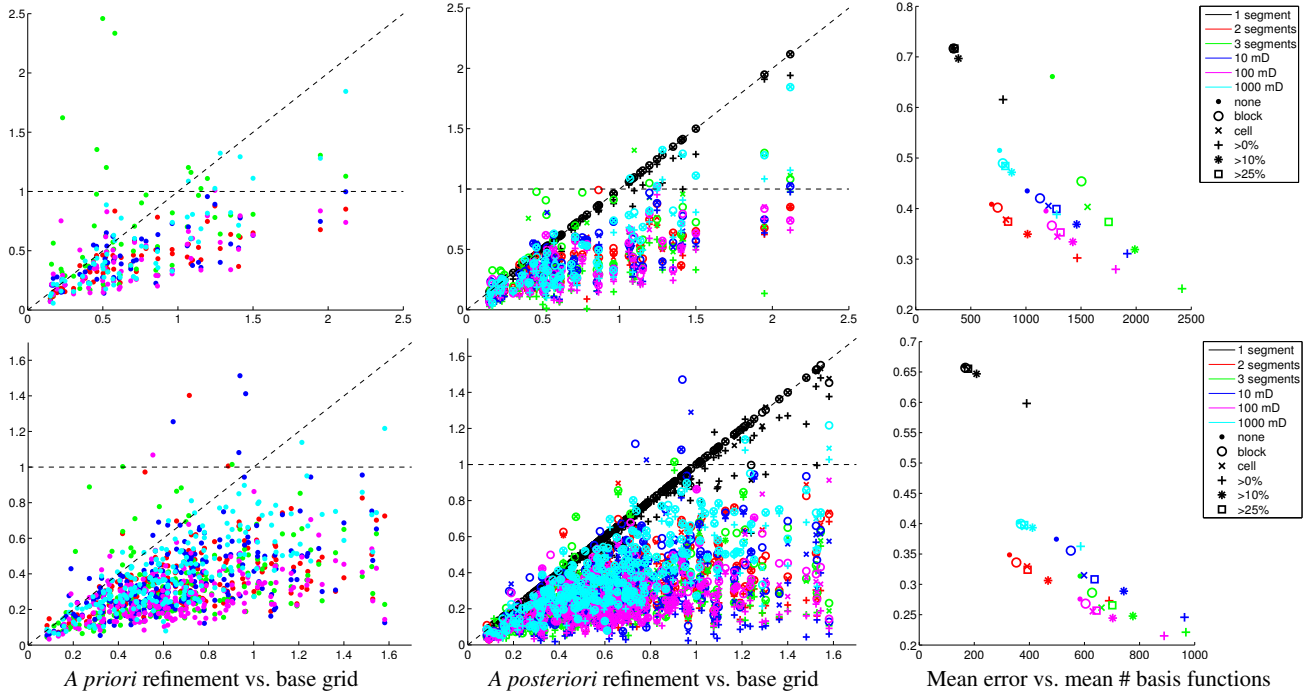


**Fig. 8** Comparison of  $L^1$  error in coarse fluxes computed by DNR for  $x$ -slices of SPE10 with analytic boundary conditions (upper row) and  $y$  slices with linear pressure boundary conditions (lower row). The left column shows cross-plots of grids with different *a priori* refinement versus the base unrefined grid, whereas the middle column shows similar plots for grids created by combining *a priori* and *a posteriori* refinements. In the plots, colors signify *a priori* refinement type, whereas markers give *a posteriori* refinement type. The plots in the right column show the mean error over all slices versus the corresponding mean number of basis functions for each grid type derived by combining different *a priori* and *a posteriori* face refinements.

- the base grid with faces subdivided into subfaces according to foreground and background permeability (denoted 'fNUC');
- the base grid with a  $2 \times 2$ ,  $5 \times 5$ , or  $10 \times 10$  subdivision of each face introduced only in cells that represent the foreground.

All six grids are illustrated at the bottom of Figure 9.

For the barrier cases ( $K_b$  fixed,  $K_f$  varying, left column in Figure 9), we observe very large errors for the base case ( $5 \times 5 \times 1$  coarse grid) when the media contrast spans five to seven orders of magnitude, in particular for Mask 3. Refining the faces reduces the error somewhat, and the reduction in error is almost the same regardless of what type of face refinement is introduced. In all cases, the lowest number of basis functions is obtained with nonuniform refinement, and this should therefore be our method of choice. For the high-

est media contrasts, the error is reduced significantly more if we instead perform a volumetric refinement so that the blocks adapt to the barriers. On the other hand, as the media contrast decreases, the error of the volumetric adaption increases because of numerical errors introduced by non-rectangular coarse blocks. This is particularly evident for parameter  $K_f = 1000$ , which corresponds to a homogeneous medium. Here, we clearly observe strong numerical artifacts also for grids having more than a single basis function associated with each coarse interface. One possible source of this error is that the 2-block does not reproduce uniform flow. The 1-block method, on the other hand, reproduces uniform flow but has errors that are equal or larger for all media contrasts except for the homogeneous case. (Note that the 1-block method will give lower errors if basis functions are constructed using *global boundary conditions*). This indi-

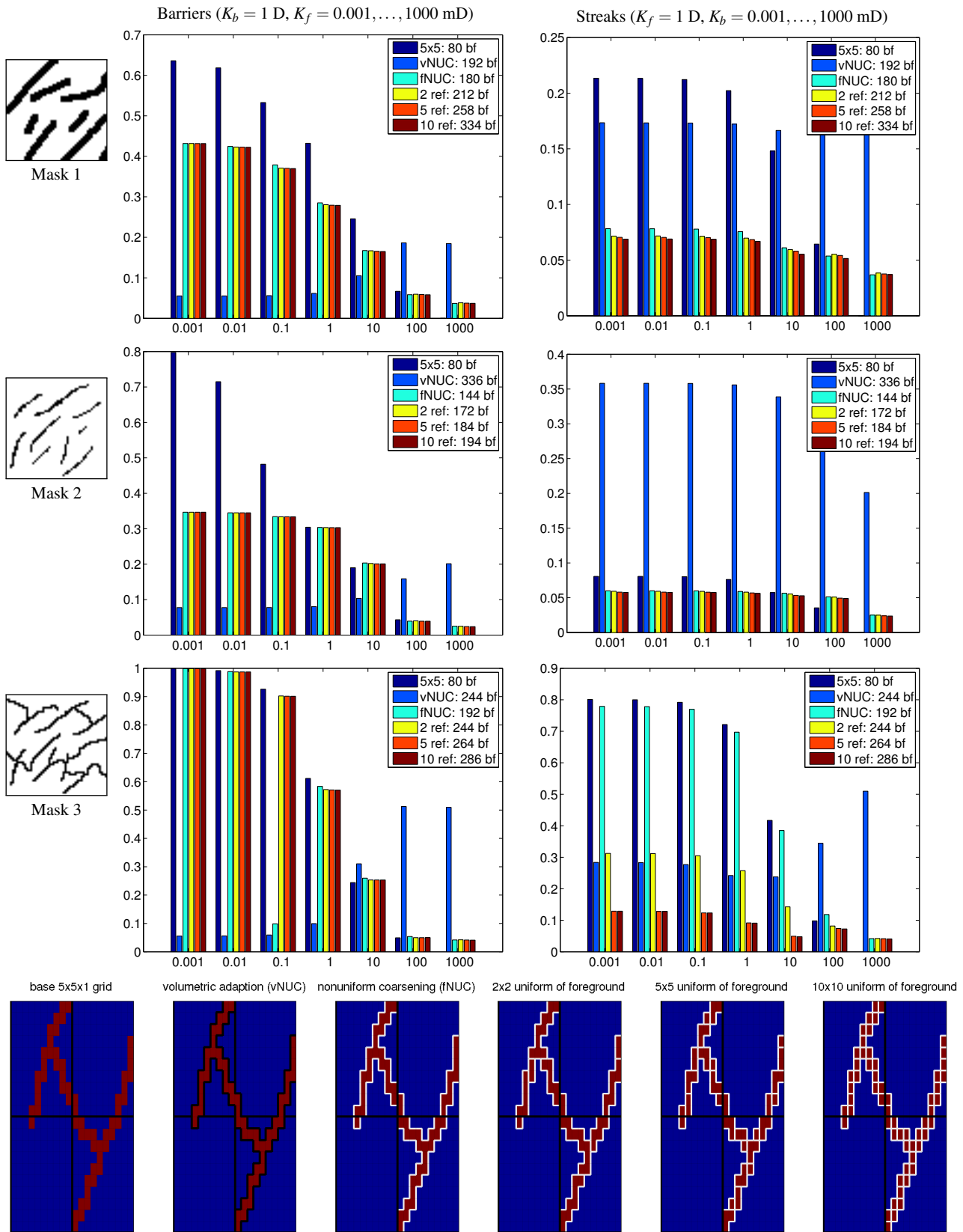


**Fig. 9** Relative  $L^1$  error in coarse-scale fluxes for the 2-block MsMFE method for a set of cases with barriers or high-permeable streaks (as function of  $K$  in units milli darcy). The small plots in the left column show the permeability masks with black color denoting the foreground permeability and white color denoting the background permeability. The lower plots show a 2D zoom of the six different grids used in the experiment: red color is foreground permeability, black color is coarse-block faces before subdivision, and white color subdivision lines.

cates that boundary conditions and geometrical complexity of the coarse blocks may be more important sources of errors than the inability to produce uniform flow. The increase in error is also most pronounced for Mask 3, for which the streaks have the most complicated geometry.

Moving on to the case with high-permeable streaks (right column in Figure 9), we first of all observe that the volumetric subdivision is clearly unsuitable. This is particularly evident for Mask 2, in which the cells inside the streaks in many places are only connected through edges (and not faces). This will result in a large number of coarse blocks and an overall set of basis functions that does not produce the almost linear pressure in a good way. Secondly, it does not seem to matter much what type of face refinement one chooses for the two first masks. For Mask 3, subdividing faces according to foreground and background permeability gives surprising small reduction in the error and further subdivision of the high-permeability streaks is needed to reduce the error.

We have not yet been able to implement the DNR method with arbitrarily shaped subface partitions, and hence we were not able to run the method for the setup discussed in this example.

*Example 6 (2D PEBI)* In this example, we will consider barriers and high-permeable streaks modeled on a 2D unstructured perpendicular bisector (PEBI) grid supplied with four different permeability realizations:

- barrier configuration as in the previous example using Mask 3 with  $K_f = 1$  mD and  $K_b = 1$  D;
- high-permeable streak using Mask 3 with  $K_b = f$  D and  $K_f = 1$  mD;
- lognormal permeability;
- lognormal permeability with low-permeable barriers from Mask 3 ( $K_f = 0.01$  mD).

A linear pressure drop from 500 to 100 bar is specified at the outer boundaries. The grid is partitioned as in Example 2: (i) an almost uniform grid obtained by sampling from a  $5 \times 5$  Cartesian partition, and (ii) a  $k$ -way Metis partition [15] with 25 blocks. In addition, three types of face refinements are applied:

- face refinement obtained by intersecting the  $5 \times 5$  base grid by a  $10 \times 10$  and a  $20 \times 20$  grid;
- face refinement obtained by intersecting the 25 block Metis partition by a 50 block and a 100 block Metis partition, respectively;
- using a permeability threshold of 100 mD to subdivide coarse faces.

Figure 10 reports a comparison of various face refinements for the barrier and streak cases. For the barrier cases, the lowest error is obtained if the faces are adapted to fit the barrier exactly ('100 mD' in the figure). For high-permeable

streaks, the 2-block method still has its lowest error when the grid is adapted to the high-permeable streaks, whereas the DNR method has the lowest error for refinements that do not adapt to the structure of the permeability field.

Figure 11 reports a similar refinement study for the last two permeability models. Here, we also use two new types of face refinement:

- face refinement by intersecting the coarse grid with another 'flow-adapted' coarse grid [9] with permeability as flow indicator ('fNUC');
- subdividing coarse faces by grouping the permeabilities into four bins using threshold values 10, 100, 1000 mD.

With only lognormal permeability, we observe three interesting trends: (i) uniform partitions systematically give higher accuracy than Metis partitions; (ii) whereas a uniform face partition improves the DNR solutions, nonuniform partitions adapted to the permeability do not; and (iii) all face refinements *increase* the error for the 2-block method. If barriers are added, the flow will to a large extent be dictated by the low-permeable barriers and the best accuracy is obtained if we add face refinement that adapts to the barriers using either a single threshold value of 10 mD or a partition of permeability into four levels.

## 6 Concluding remarks

We have presented two new methodological developments. First, the Dirichlet–Neumann representation (DNR) method [20] has been extended to fully unstructured grids in 2D. Second, the MsMFE method [7] has been extended to coarse grid with subdivided faces so that more than one basis function may be associated with each pair of coarse blocks. The 2-block formulation of the MsMFE method does not reproduce constant flow when coarse faces are subdivided. Subdividing coarse faces will therefore not improve the error if the flow field has a dominant linear component. Likewise, the DNR method only reproduces constant flow if extra segments one cell wide are added at each vertex of the coarse grid. The 1-block MsMFE method reproduces constant flow by design, which is important for smooth heterogeneities, but may be less important for channelized and high-contrast media. However, we believe that essential features of the fix for constant flow should be reflected when extending the DNR method to 3D. In particular, face pressure boundary conditions should not form global smooth functions over non-manifold coarse cell boundaries.

We have performed an extensive series of numerical experiments both for synthetic and realistic cases; a few have been reported herein and more results can be found in [17, 11]. In summary, the results show that subdividing coarse faces to capture high-flow effects will increase the resolution of the DNR and the MsMFE methods for cases with

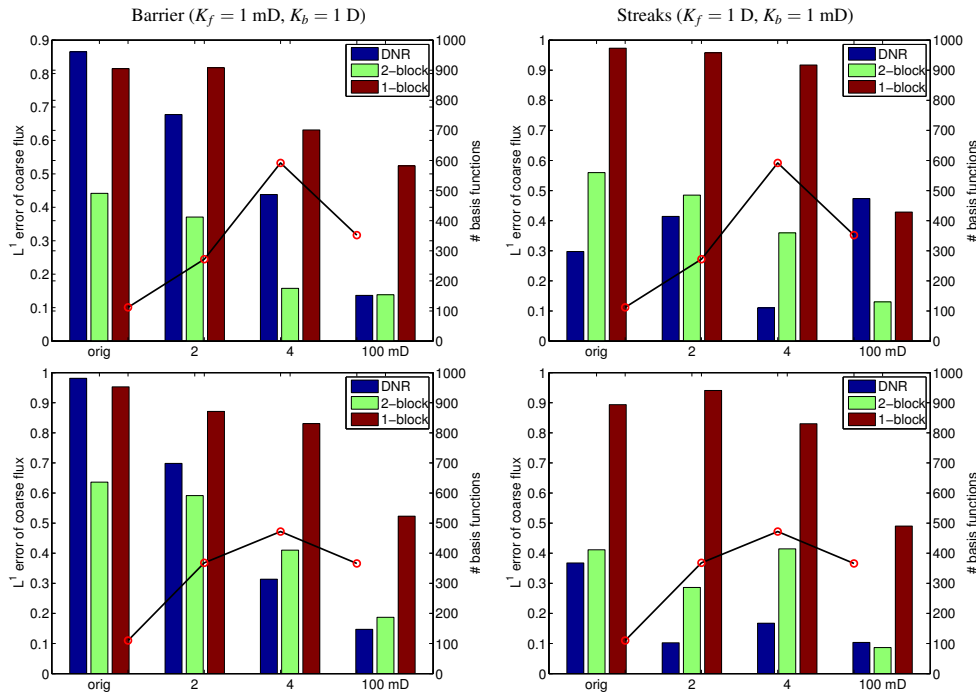


**Fig. 10** Barriers and high-permeable streaks for Mask 3 modeled on a 2D PEBI grid. The bars show  $L^1$  errors for the coarse-scale fluxes and the lines with markers show the number of blocks involved in the computation of basis functions for various types of face refinement for the DNR and the two MsMFE methods. In the upper row, we use a  $5 \times 5$  coarse partition and in the lower row a 25 block Metis partition.

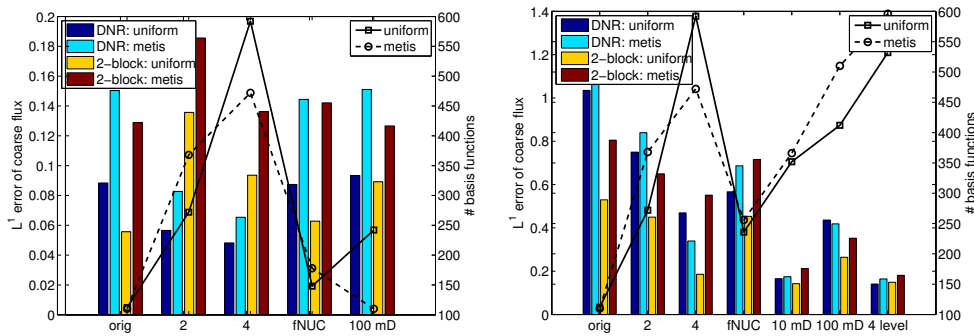


**Fig. 11** The left plot shows a comparison of face refinement for uniform and Metis partitions for a model with lognormal permeability and linear pressure. The right plot shows a similar lognormal model with low-permeable barriers (0.01 mD) imposed according to Mask 3.

flow *across* regions of strong contrasts. Barriers and other no-flow effects, on the other hand, where the flow is *confined* by media contrasts, are captured more accurately by using volumetric grid adaption. Altogether, the DNR and 2-block MsMFE methods are quite robust and generally produce low errors compared with standard upscaling methods. The 1-block MsMFE method with local boundary conditions is less accurate than the other two methods, but will generally be *more robust and accurate* if global boundaries are used to compute basis functions. All three methods will occasionally lead to large errors for specific coarse grids, possibly in combination with face refinements. One solution to cure this problem would be to use *a posteriori* adaption; a simple approach in this direction was presented for subsets of the SPE10 data set. In practice, it may be possible to use a combination of user experience and/or geological knowledge to introduce adaption in targeted areas only. Likewise, global fine-scale information (e.g., based on generic boundary conditions) may be available and can be used to guide

the subdivision of faces or to set global boundary conditions for the 1-block MsMFE method.

The results reported herein complements previous comparisons of multiscale and upscaling methods, e.g., as reported in [13], and shows that it is generally difficult to pick one particular multiscale-type method or gridding approach that is more robust than others. In our experience, one can always construct cases for which a particular method performs better or worse than a set of alternative methods. Nevertheless, we have tried to summarize the experience we have gained by running a large number of cases of the type reported herein in the following guidelines:

- use volumetric refinement for flows that mostly take place with high-permeable (or low-permeable) regions;
- use face refinement when there is much flow across high permeability contrasts;
- perform simulations on more than one coarse grid; both the DNR and the MsMFE method may give large errors for specific coarse grids;

- *a posteriori* refinement of blocks or block faces can have a modest cost and will improve accuracy in many cases.

The guidelines are admittedly not very precise. In our experience, picking the right method and designing the best grid, which is optimal with respect to both accuracy and runtime, is more an art than a precise science with the current state-of-the-art.

**Acknowledgements** The authors are grateful to Adedayo Oyerinde for helpful discussions.

## References

1. Aarnes, J., Lie, K.A.: Toward reservoir simulation on geological grid models. In: Proceedings of the 9th European Conference on the Mathematics of Oil Recovery. EAGE, Cannes, France (2004)
2. Aarnes, J.E.: On the use of a mixed multiscale finite element method for greater flexibility and increased speed or improved accuracy in reservoir simulation. *Multiscale Model. Simul.* **2**(3), 421–439 (electronic) (2004)
3. Aarnes, J.E., Kippe, V., Lie, K.A.: Mixed multiscale finite elements and streamline methods for reservoir simulation of large geomodels. *Adv. Water Resour.* **28**(3), 257–271 (2005)
4. Aarnes, J.E., Krogstad, S., Lie, K.A.: A hierarchical multiscale method for two-phase flow based upon mixed finite elements and nonuniform coarse grids. *Multiscale Model. Simul.* **5**(2), 337–363 (electronic) (2006)
5. Aarnes, J.E., Krogstad, S., Lie, K.A.: Multiscale mixed/mimetic methods on corner-point grids. *Comput. Geosci.* **12**(3), 297–315 (2008). DOI 10.1007/s10596-007-9072-8
6. Arbogast, T.: Homogenization-based mixed multiscale finite elements for problems with anisotropy. *Multiscale Model. Simul.* **9**(2), 624–653 (2011). DOI 10.1137/100788677
7. Chen, Z., Hou, T.: A mixed multiscale finite element method for elliptic problems with oscillating coefficients. *Math. Comp.* **72**, 541–576 (2003)
8. Christie, M.A., Blunt, M.J.: Tenth SPE comparative solution project: A comparison of upscaling techniques. *SPE Reservoir Eval. Eng.* **4**, 308–317 (2001). Url: <http://www.spe.org/csp/>
9. Hauge, V.L.: Multiscale methods and flow-based gridding for flow and transport in porous media. Ph.D. thesis, Norwegian University of Science and Technology (2010). URL <http://ntnu.diva-portal.org/smash/get/diva2:400507/FULLTEXT02>
10. Hauge, V.L., Lie, K.A., Natvig, J.R.: Flow-based coarsening for multiscale simulation of transport in porous media. *Comput. Geosci.* **16**(2), 391–408 (2012). DOI 10.1007/s10596-011-9230-x
11. Høyland, A.G.: Multiscale methods in reservoir simulation. Master's thesis, University of Bergen (2012)
12. Jenny, P., Lee, S.H., Tchelepi, H.A.: Multi-scale finite-volume method for elliptic problems in subsurface flow simulation. *J. Comput. Phys.* **187**, 47–67 (2003)
13. Kippe, V., Aarnes, J.E., Lie, K.A.: A comparison of multiscale methods for elliptic problems in porous media flow. *Comput. Geosci.* **12**(3), 377–398 (2008). DOI 10.1007/s10596-007-9074-6
14. Lie, K.A., Krogstad, S., Ligaarden, I.S., Natvig, J.R., Nilsen, H.M., Skaflestad, B.: Open source MATLAB implementation of consistent discretisations on complex grids. *Comput. Geosci.* **16**, 297–322 (2012). DOI 10.1007/s10596-011-9244-4
15. Metis – serial graph partitioning and fill-reducing matrix ordering (2012). Url: <http://glaros.dtc.umn.edu/gkhome/views/metis>
16. The MATLAB Reservoir Simulation Toolbox, version 2011b (2012). <http://www.sintef.no/MRST/>
17. Natvig, J.R., Lie, K.A., Krogstad, S., Yang, Y., Wu, X.H.: Grid adaption for upscaling and multiscale methods. In: Proceedings of ECMOR XIII–13th European Conference on the Mathematics of Oil Recovery. EAGE, Biarritz, France (2012)
18. Natvig, J.R., Skaflestad, B., Bratvedt, F., Bratvedt, K., Lie, K.A., Laptev, V., Khataniar, S.K.: Multiscale mimetic solvers for efficient streamline simulation of fractured reservoirs. *SPE J.* **16**(4) (2011). DOI 10.2018/119132-PA
19. Nilsen, H.M., Lie, K.A., Natvig, J.R.: Accurate modelling of faults by multipoint, mimetic, and mixed methods. *SPE J.* **17**(2), 568–579 (2012). DOI 10.2118/149690-PA
20. Yang, Y., Li, D., Parashkevov, R., Wu, X.H.: A Dirichlet Neumann representation method for simulating flows in reservoirs. In: 2011 SPE Reservoir Simulation Symposium, The Woodlands, Texas, USA, 21-23 February 2011 (2011). DOI 10.2118/141512-MS